Optical Trirefringence in Photonic Crystal Waveguides

M. C. Netti, A. Harris, and J. J. Baumberg

Department of Physics & Astronomy, University of Southampton, SO17 1BJ, United Kingdom

D. M. Whittaker

Toshiba Research Europe, Ltd., Cambridge, CB4 4WE, United Kingdom

M. B. D. Charlton, M. E. Zoorob, and G. J. Parker

Department of Electronics & Computer Science, University of Southampton, Southampton SO17 1BJ, United Kingdom

We demonstrate that 2D photonic crystals can possess optical trirefringence in which there are six field orientations for which linear incident light is not perturbed on reflection or transmission. Such a property is rigorously forbidden in homogeneous nonmagnetic dielectrics which can possess only optical birefringence. We experimentally demonstrate this phenomena in silicon-based mesostructures formed from photonic crystal waveguides embedded in a Fabry-Perot cavity. Multirefringence is controlled by the presence of submicron dielectric patterning and is well explained by an exact scattering matrix theory.

Optical polarization phenomena associated with the anisotropy of natural crystals have been a source of intrigue for centuries. In 1672 the Dutch physicist Christiaan Huygens showed that the two beams arising from double refraction in calcite have orthogonal polarizations [1], subsequently used by Nicol to make *birefringent* polarizers [2]. The realization that light can travel in the same direction but with different speeds depending on the different orientation of the transverse electric field was one of the early successes of optics predicted by Maxwell's equations [3]. A central result of this treatment is that no matter how anisotropic the underlying crystal structure is, transparent dielectrics can possess at most two refractive indices for any propagation direction, which must be oriented along two principal axes at 90° to each other. This familiar arrangement of different refractive indices mutually at right angles now forms the basis of an extensive array of optoelectronic polarization technologies.

Here we report the first evidence for optical *multi-refringence*, using a new class of mesophotonic materials which have been patterned on the scale of the optical wavelength. Much recent work has focused on the photonic band gap properties of materials patterned in 1, 2, and 3 dimensions [4–9]. These new optical materials exhibit a whole range of phenomena that require the traditional intuitive laws of optics to be revised, for instance superprism and superrefraction effects [10]. In the present work, a 2D photonic crystal waveguide is incorporated in a Fabry-Perot cavity and the coupling to light examined. Sharp resonances are observed in the reflectivity which correspond to scattering into lossy waveguide modes within the structure. By rotating the sample about the nanopatterned input face, clear evidence is seen for six principal polarization axes along which the electric field polarization is not mixed, arranged at 60° separations. The origin of this trirefringence [11] is the extreme mixing of polarizations that can occur within the nanopatterned layers, and is well described by a scattering matrix model.

If the response of a transparent dielectric to an optical field can be parametrized by the dielectric tensor $\underline{\boldsymbol{\varepsilon}}$ (i.e., nonmagnetic, homogeneous, and lossless) where $\underline{\mathbf{D}} = \underline{\boldsymbol{\varepsilon}}\mathbf{E}$, then a strong theorem due to time reversal symmetry insists that the $\underline{\boldsymbol{\varepsilon}}$ is Hermitian [3]. Maxwell's equations can then be simply written in an orthogonal principal coordinate system (so that $\underline{\boldsymbol{\varepsilon}}$ is diagonal) resulting in perpendicular optic axes whatever the underlying crystal symmetry and the direction of propagation [3]. The use of uniaxial/biaxial crystals and waveguides is crucial for the operation of many polarization optical components. The property of orthogonal principal axes is universal, until the wavelength of radiation is reduced down to the atomic spacing (e.g., x-ray, TEM). Thus it is clear that patterning materials on the scale of the wavelength of the fields can modify their birefringent properties.

In order to demonstrate how mesoscale photonic materials radically redefine the conventional laws of optics, reflection measurements were performed on photonic crystal (PC) waveguides embedded in a Fabry-Perot cavity. Because the Fresnel reflection and transmission coefficients are angle dependent, clear manifestations of this multirefringent behavior must occur without changes in inclination of any interfaces in the measurements. For that reason we study light propagation through a microstructured sample which is rotated about the normal to its surface plane, and monitor the polarization dependent reflectivities as in ellipsometry [Fig. 1(a)]. The waveguide layers consisted of a low pressure chemical vapor deposited Si_3N_4 slab ($n_1 = 2.02$, $d_1 = 250$ nm) sandwiched between two layers of silicon dioxide SiO_2 ($d_0 = 120$ nm cladding, $d_2 = 1.73$ μm spacer, $n_2 = 1.46$) [12]. A triangular lattice of air rods defined by electron-beam lithography was etched 370 nm down into the spacer layer in order to create a periodic slab
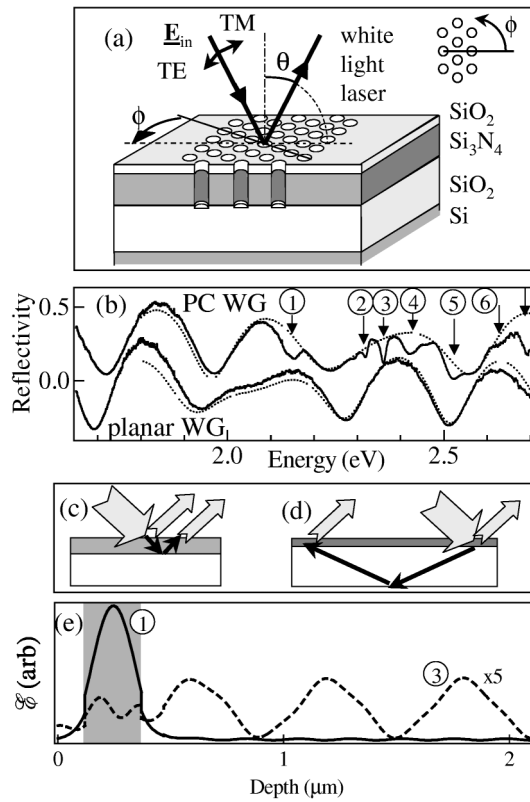
FIG. 1. (a) Schematic reflectivity experiment, showing the orientation of the fields (polar angle θ, azimuthal angle ϕ) and the sample design. (b) Reflectivity of patterned and unpatterned waveguide (solid) with fits to Fabry-Perot fringes (dotted). The new resonances are marked 1–6 [(c),(d)]. Ray paths for modes 1,3 respectively. (e) Intensity profiles vs depth of modes 1 and 3, averaged over time and in-plane coordinates.

of PC with good uniformity. The triangular lattice consisted of 256 rows of air columns with a pitch, $\Lambda = 300$ nm and a pore radius of 75 nm. This choice of the air-filling fraction $f = 0.23$ was previously optimized for deep photonic band gaps in the near infrared ranges ($\lambda_{\text{gap}} = 780$–$850$ nm) [13].

To simplify the measurement of the 64 μm wide patterned region, a white light laser was exploited, focused to a 50 μm spot on the investigated samples. The ultrabroadband white light continuum was produced by focusing the 5 μJ output of a 100 fs regenerative amplifier through a sapphire plate. Achromatic polarization and focusing optics were employed, and the far-field collimation improved using photonic-crystal fiber as described previously [13]. The reflectance was obtained by simultaneously recording the input beam spectrum and the reflected signal.

A typical reflectance spectrum shown in Fig. 1(b) (incident angle $\theta = 47°$, azimuthal angle $\phi = 12°$, TE) reveals the presence of a number of sharp modes (dips) superimposed on a background of Fabry-Perot (FP) fringes. The top (air/SiN) and bottom (SiO/Si) cavity interfaces form a low-finesse cavity responsible for the weak periodic modulation. The appearance of closely spaced sharp modes has not been previously seen but is, however, predicted by our theoretical model [14]. The first modes originate from the lowest order TE waveguide (WG) mode in the SiN photonic crystal, while the closely spaced higher-energy modes (2)–(6) result from PC-induced coupling to glancing-angle Fabry-Perot modes strongly confined in the SiO spacer layer (termed "quasi-WG" modes). The scattering matrix theory, which incorporates a 2D plane wave expansion in the patterned layers, provides field profiles that confirm this analysis [Fig. 1(e)]. Both PC waveguide and quasi-WG resonances can be understood from the zone folding of their in-plane mode dispersions due to the periodic patterning [Fig. 2(a)].

The modification of reflectivity is due to the interference of these folded modes with the light reflected from the top sample surface, thus allowing the internal propagation phase inside the structure to be tracked. The mth angular condition for destructive interference from the quasi-WG mode at a resonant wavelength λ;
$$\sin\theta_m = \frac{\lambda}{b\Lambda} - \sqrt{(n_2^2 + \bar{n}_1^2 a + \bar{n}_0^2 a')/b - (\tfrac{\lambda}{b})^2[\tfrac{a+a'}{\Lambda^2} + (2m+1)^2/4]},$$
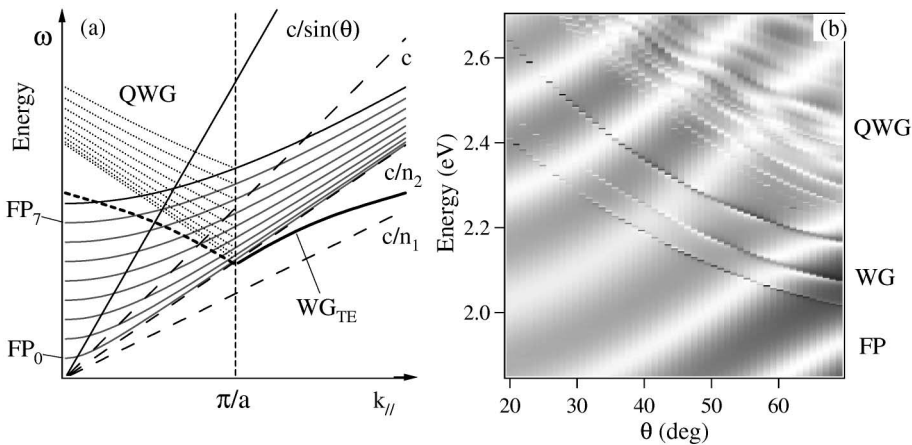

FIG. 2. (a) Effect of one-dimensional patterning on the photon dispersion in a waveguide, showing waveguide (WG) and Fabry-Perot (FP) resonances, together with the quasi-WG (QWG) modes. The periodicity introduces band gaps (not shown) and zone folding allowing an interrogating probe incident at θ on the sample to scatter into these lossy modes. (b) Full scattering matrix calculation of the reflectivity spectra vs θ (maximum R is dark), showing both FP, WG, and QWG resonances. $\phi = 10°$, TE$_{\text{in/out}}$.

where $a = d_1/d_2, a' = d_0/d_2, b = 1 + a + a'$. While the full model [Fig. 2(b)] considers exactly refraction in the PC layer, the analytic model assumes $\bar{n}_{0,1}$ to be given by the effective volume-averaged refractive indices for the patterned WG layers. As the angle of incidence θ increases, the WG and quasi-WG modes *drop* in energy in contrast to the FP modes, as predicted by the zone folding of the bands.

Using achromatic wave plates and polarizers, both TE and TM are separately used for the input and output probe polarizations. The photonic band gaps in this sample lie at much lower energy than the near zone-center photonic modes examined in reflectivity [Fig. 3(a)] [13]. Measurements for the TE_{in}/TE_{out} and TM_{in}/TM_{out} conditions [Figs. 3(b) and 3(c)] are well accounted for by the full theoretical model [Fig. 3(e)]. The TE polarization shows greater contrast due to the stronger Fresnel coefficients at each interface within the structure. For incident orientations which do not line up exactly with the triangular lattice ($\phi \neq n\frac{\pi}{6}$), two low-energy resonances are seen in the reflectivity with one dominant for each of the polarization conditions. Close to $\phi = 0°$, the lower of the two resonances is seen in TM/TM, while the upper mode is seen in
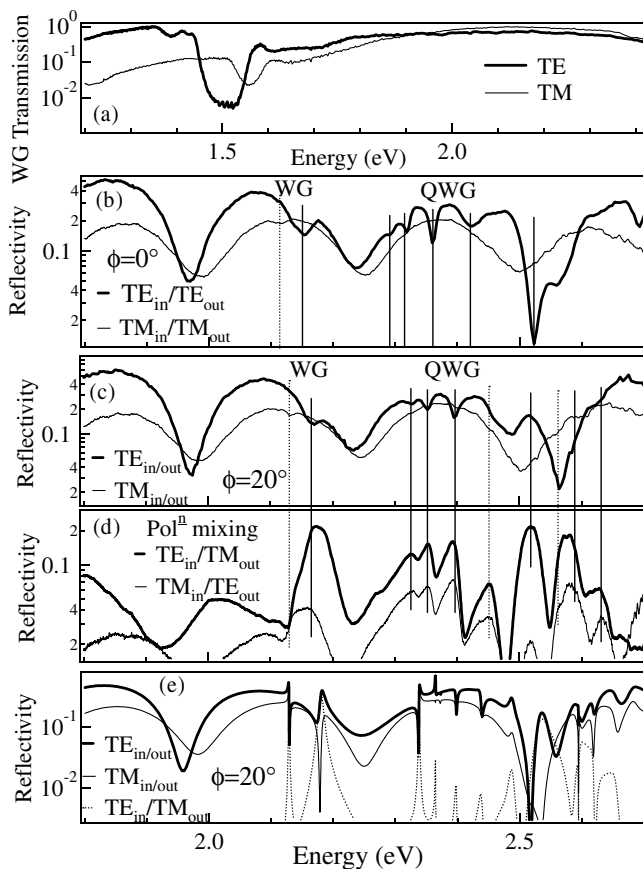

FIG. 3.   (a) In-plane WG transmission showing the photonic band gaps at lower energy. (b),(c) Reflectivity at $\theta = 47°, \phi = 0, 20°$ for TE_{in}(TM)$/TE_{out}$(TM) showing the splitting of the lowest WG mode. Solid (dashed) lines mark TE (TM) resonances. (d) Reflectivity at $\phi = 20°$ for TM_{in}(TE$/TE_{out}$(TM) showing the polarization mixing enhanced at the resonance energies. (e) Theoretical simulation of the polarization mixing.

TE/TE. As ϕ approaches 30° this distribution reverses. The two resonances originate from the different effective refractive indices seen by different standing waves leading to splitting away from the zone center [15]. The separation between these modes (35 meV) corresponds to the splitting induced by coupling between propagating WG modes with different symmetries. Although the model predicts strong enhancements of the reflectivity up to 100%, negative dips are observed more clearly in the data. We believe that this is not caused by an experimental artifact since no combination of averaging over θ, Λ, or f produces a better fit to the results. The strong reflection enhancement and the ultrasharp predicted dips depend on the assumed infinite lifetime of the PC-WG mode inside the waveguide, whereas in practice the lifetime is reduced by enhanced scattering losses in the SiN perforated layer. In addition, the angular dispersion of the modes, coupled with the finite size of the structure and the range of incident angles ($\Delta\theta \sim 2°$), contribute to smear the sharp resonances. The observation of both the PC-WG and quasi-WG resonances demonstrates the rich variety of mode engineering possible in these photonic-crystal-clad Fabry-Perot cavity structures. For a planar unpatterned waveguide, no polarization mixing is possible between the TE and TM modes — whichever field direction is incident on the WG, it remains in this orientation on reflection. This property is broken by the addition of mesoscale photonic patterning, and light incident as TE can emerge with TM polarization [Fig. 3(d)], strongly enhanced at each of the reflection resonances. This polarization rotation is absent for light polarized along the principal axes of the structure, which in this case occurs for in-plane angles $\phi = n\frac{\pi}{6}$. Away from these symmetry directions, strong polarization rotations up to 20° are seen. Thus mesophotonic materials can possess *multirefringence*, breaking the condition demanding *orthogonal* normal modes for propagation in a transparent dielectric.

The 60° symmetry arises from the ϕ-dependent dispersion in the photonic crystal. The resonances observed are strongly dependent on the in-plane direction of the incident light with reference to the triangular lattice. Data taken through $0° < \phi < 180°$ at a spacing of 2.5° are shown as an $E - \phi$ image in Figs. 4(a) and 4(b), revealing a similar nonmonotonic shift for all the modes. Extracting the energies of the first three peaks results in Fig. 4(c), which clearly demonstrates the zone folding and this sixfold symmetry. Because the polarization mixing is enhanced at the same resonance energies, it follows a similar orientation dependence. The polarization rotation both measured and calculated is shown as a function of ϕ in Figs. 4(d) and 4(e).

We note that detailed balance insists that the mixing from TE to TM must equal that from TM to TE. The triangular-lattice clad Fabry-Perot thus produces *two* principal refractive indices, distributed between *six* normal polarization modes. Trirefringence implies *three* refractive indices. A careful inspection of Fig. 4(c) reveals that the minimum energies of the resonant modes are not the same along the three principal axes. The cause is a slight imbalance in
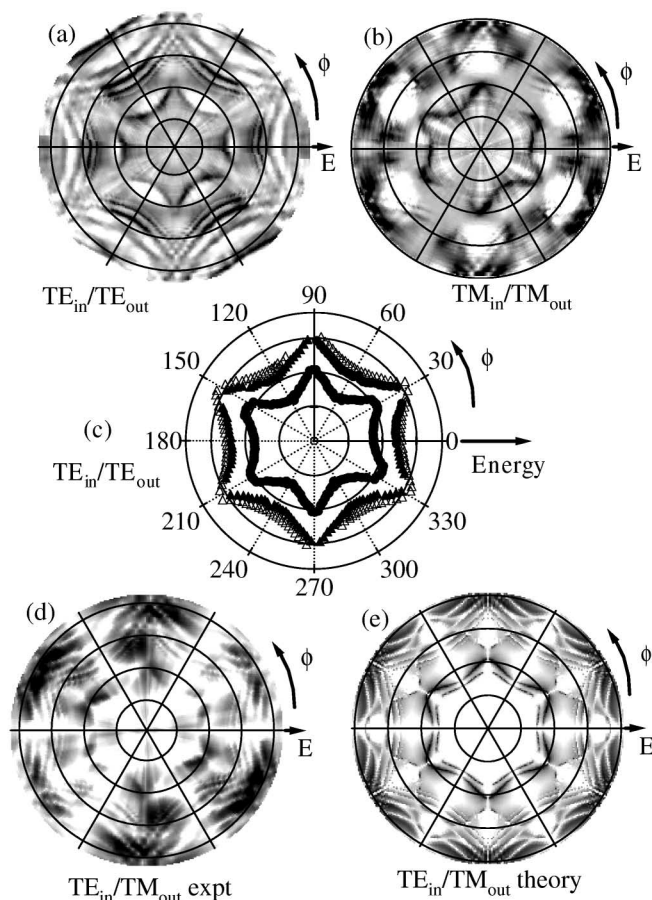
FIG. 4.   Polar image plots of the reflectivity spectra (dark corresponds to small R) vs energy (radially, concentric circles at $E = 2.0$, 2.2, 2.4, and 2.6 eV) and in-plane hole orientation ($\phi = 0-180°$ measured, $180°-360°$ by symmetry, and independently checked). (a) TE_{in}/TE_{out}, (b) TM_{in}/TM_{out}, showing the ϕ dispersion and redistribution of mode strengths. (c) Extracted energies of the lowest three TE_{in}/TE_{out} resonances ($\bullet$, $\blacktriangle$, $\triangle$). Experimental (d) and theoretical (e) ϕ dispersions of the polarization mixing for TE_{in}, showing good agreement in the basic symmetries and dispersions.

the spacing between holes within a row, and between the rows, developed in the discretization of the electron beam raster during the large-area lithography. Thus for the lowest WG mode, there are three distinct energies along the principal axes, $E_1(\phi = 0, \pi) \neq E_2(\phi = \frac{\pi}{3}, \frac{2\pi}{3}, \frac{4\pi}{3}, \frac{5\pi}{3}) \neq E_3(\phi = \frac{\pi}{6} + n\frac{\pi}{3})$. The magnitude of the trirefringence depends on the wavelength, the resonance widths, and the exact structure; however, theory shows that polarization rotations on reflection of up to 90° may be possible in optimized samples. Clearly patterning different PC symmetries can result in a wide variety of multirefringent properties. Polarization rotation is forbidden for light incident along directions which are lines of reflection symmetry of the structure [14]. This explains the sixfold symmetry of the principal axes—they are the symmetry axes of the ideal structure. In the present case the slight distortion of the axes should mean that there are only two symmetry axes, but the effect on the band structure is too weak

to cause measurable rotation. Reflection symmetry is affected by both the lattice and the basis (hole shape); however, the low-lying bands examined here are not highly sensitive to the shape of the hole, so the major effect is due to the lattice symmetries. The square photonic lattice, previously the subject of considerable attention [15], however does not show this property because its symmetry matches that of the incident linear polarization. One-dimensional gratings above waveguides exhibit similar quasi-WG resonant modes [5,16] resulting in birefringence only in large amplitude gratings. However, they do not generate the sixfold polarization axes observed here. The trirefringent property arises directly here from the symmetry of the underlying lattice, enabling a new range of optical components with modified polarization properties. For instance, we are currently investigating dodeca-refringence in our photonic quasicrystal waveguides [8].

[1] C. Huygens, *Traité de la Lumière* (Van der Aa, Leiden, 1690).
[2] W. Nicol, Edinburgh New Phil. J. **6**, 83 (1829).
[3] M. Born and E. Wolf, *Principles of Optics* (Cambridge University Press, Cambridge, England, 1999).
[4] J. D. Joannopoulos, R. D. Meade, and J. N. Winn, *Photonic Crystals* (Princeton University Press, Princeton, New Jersey, 1995).
[5] P. St. J. Russell *et al.,* in *Microcavities and Photonic Bandgaps,* edited by J. Rarity and C. Weisbuch (Kluwer, The Netherlands, 1996).
[6] T. F. Krauss, R. M. De La Rue, and S. Brand, Nature (London) **383**, 699 (1996).
[7] E. Yablonovitch, Phys. Rev. Lett. **58**, 2059 (1987).
[8] M. E. Zoorob *et al.,* Nature (London) **404**, 740 (2000).
[9] S. G. Johnson *et al.,* Phys. Rev. B **60**, 5751 (1999).
[10] H. Kosaka *et al.,* Phys. Rev. B **58**, R10 096 (1998); H. Kosaka *et al.,* Appl. Phys. Lett. **74**, 1212 (1999); H. Kosaka *et al.,* Phys. Rev. B **62**, 1477 (2000).
[11] The word *birefringence* can refer to *two* optic axes or *two* refractive indices—the maximum exhibited by anisotropic crystals. We use *trirefringence* to denote three refractive indices. Symmetry forbids only three optic axes—six optic axes are observed here (a multiaxial symmetry). An alternative meaning for birefringence is that *two* waves propagate in different directions inside the crystal—in this context photonic crystals are multirefringent since the number of internal waves propagating depends on the number of photonic bands excited.
[12] M. B. D. Charlton, S. W. Roberts, and G. J. Parker, Mater. Sci. Eng. B **49**, 155 (1997).
[13] M. C. Netti *et al.,* Appl. Phys. Lett. **76**, 991 (2000).
[14] D. M. Whittaker and I. S. Culshaw, Phys. Rev. B **60**, 2610 (1999); V. N. Astratov *et al.,* Appl. Phys. Lett. **77**, 178 (2000).
[15] P. Paddon and J. F. Young, Phys. Rev. B **61**, 2090 (2000).
[16] D. Rosenblatt, IEEE J. Quantum Electron. **33**, 2038 (1997).